american physiological society

JNP JOURNAL OF NEUROPHYSIOLOGY

J Neurophysiol 135: 747–759, 2026.
First published February 5, 2026; doi:10.1152/jn.00396.2025

RESEARCH ARTICLE

Sensory Processing

Characteristics of cross-modal negative BOLD responses in the human sensory subcortex and cortex

Toshikazu Miyata,[1,2,3] Masaki Fukunaga,[4,5,6] Junxiang Luo,[1,5,6] Isao Yokoi,[1,7] Tetsuya Yamamoto,[4,6] Ayumi Yoshioka,[4,8] Jiajia Yang,[9] Tomoyo Morita,[10,11] and Hiromasa Takemura[1,2,5,6]

[1]*Division of Sensory and Cognitive Brain Mapping, Department of System Neuroscience, National Institute for Physiological Sciences, Okazaki, Japan;* [2]*Department of Quantitative and Imaging Biology, Headquarters for Co-Creation Strategy, National Institutes of Natural Sciences, Tokyo, Japan;* [3]*Princeton Neuroscience Institute, Princeton University, Princeton, New Jersey, United States;* [4]*Section of Brain Function Information, National Institute for Physiological Sciences, Okazaki, Japan;* [5]*Graduate Institute for Advanced Studies, SOKENDAI, Hayama, Japan;* [6]*Core for Spin Life Sciences, Okazaki Collaborative Platform, National Institutes of Natural Sciences, Okazaki, Japan;* [7]*Technical Division, National Institute for Physiological Sciences, Okazaki, Japan;* [8]*Research Organization of Science and Technology, Ritsumeikan University, Kusatsu, Japan;* [9]*Graduate School of Interdisciplinary Science and Engineering in Health Systems, Okayama University, Okayama, Japan;* [10]*Center for Information and Neural Networks (CiNet), Advanced ICT Research Institute, National Institute of Information and Communications Technology (NICT), Suita, Japan; and* [11]*Graduate School of Frontier Biosciences, Osaka University, Suita, Japan*

Abstract

Functional magnetic resonance imaging (fMRI) is a noninvasive method for measuring human brain activity based on blood oxygenation level-dependent (BOLD) responses. Although many studies have reported positive BOLD responses evoked by sensory stimuli, others have reported negative BOLD responses (NBRs) in the sensory cortex when stimuli from different sensory modalities are presented (i.e., cross-modal NBRs). We conducted an fMRI experiment to better understand the characteristics of cross-modal NBRs in subcortical and cortical regions. Auditory and visual stimuli were presented unilaterally to one ear and to either the left or right visual field, respectively. The lateral geniculate nucleus and medial geniculate nucleus did not show a significant cross-modal NBR. In contrast, the primary auditory cortex showed a significant cross-modal NBR when visual stimuli were presented in either the contralateral or ipsilateral visual fields. Finally, we found that the cross-modal NBR in the early visual cortex was highly variable across subjects and did not exhibit consistent trends. However, each subject's data exhibited considerable split-half reliability. Our results suggest that cross-modal NBR in the auditory cortex likely reflects mechanisms such as interhemispheric suppression, rather than those coordinated within the same hemisphere.

NEW & NOTEWORTHY This study demonstrated that the human primary auditory cortex showed a significant cross-modal negative BOLD response bilaterally, regardless of the visual field in which the visual stimuli were presented. This result suggests that the cross-modal negative BOLD response is not an epiphenomenon of visual cortex activation predominantly observed in the contralateral hemisphere, but is more likely to reflect interhemispheric suppression mechanisms.

auditory system; cross-modal; functional MRI; visual system

INTRODUCTION

Humans and animals achieve adaptive behaviors by receiving environmental information through multiple sensory modalities. These diverse sensory modalities play complementary roles in identifying information from the environment, as each modality is sensitive to different types of information. Understanding how the human brain processes information from multiple sensory modalities is essential for elucidating how humans obtain crucial

Correspondence: T. Miyata (tm2158@princeton.edu).
Submitted 8 August 2025 / Revised 19 October 2025 / Accepted 29 January 2026

information from multisensory inputs to achieve adaptive behavior (1, 2) and how dysfunction in one modality impacts neural processing in other modalities (3–5). Functional magnetic resonance imaging (fMRI) is an essential method for such investigations because it enables the noninvasive measurement of blood oxygenation level-dependent (BOLD) responses, which reflect brain activity, with a relatively high spatial resolution (6). To date, fMRI studies have successfully demonstrated the presence of positive BOLD responses to visual stimuli in the visual cortex (6–8) and positive BOLD responses to auditory stimuli in the auditory cortex (9).

Several previous fMRI studies have reported the occurrence of a negative BOLD response (NBR) in the sensory cortex when stimuli from different sensory modalities are presented (10–14). Specifically, these studies reported that the auditory cortex shows an NBR for visual stimuli, whereas the visual cortex shows an NBR for auditory stimuli. This phenomenon, which we hereinafter term "cross-modal NBR," can be crucial in understanding the mechanisms of processing multisensory information in the human brain. However, the mechanisms underlying cross-modal NBR are not well understood, partly because only a limited number of studies have investigated them. It remains unclear at which stage of sensory information processing cross-modal NBR occurs.

In this study, we aimed to address a few empirical research questions regarding cross-modal NBR. First, we examined whether the subcortical nuclei, the medial geniculate nucleus (MGN) and the lateral geniculate nucleus (LGN), which play essential roles in the early stages of sensory processing, are involved in the cross-modal NBR. Second, we tested whether the cross-modal NBR reflects suppression coordinated within each hemisphere (e.g., between the auditory and visual cortices in the same hemisphere) or involves interhemispheric suppression mechanisms. Finally, we performed an exploratory analysis to characterize the spatial distribution of cross-modal NBR within the visual cortex in relation to eccentricity, given that foveal and peripheral regions generally exhibit different functional properties (15).

To address these research questions, we conducted a block-design fMRI experiment in which auditory and visual stimuli were presented unilaterally to one ear and to the left or right visual field, respectively. This lateralized stimulus design allowed us to assess whether the cross-modal NBR involves interhemispheric mechanisms. Regions of interest (ROIs), including both subcortical and cortical areas, were identified in each subject's native space based on structural MRI data. We then performed a single-subject ROI analysis to evaluate the time course and percent signal change of BOLD responses in each ROI and condition.

MATERIALS AND METHODS

Subjects

Fifteen healthy adults (4 males, 11 females) aged 20–40 yr (mean age, 25.1 yr) with normal or corrected-to-normal vision participated in the magnetic resonance imaging (MRI) experiment. All subjects were recruited from the Okazaki area, which includes neighboring cities in the Aichi Prefecture, Japan. Before participating in the experiment, all subjects signed a written informed consent form that included explanations of voluntary participation, safety for the MRI experiment, freedom to withdraw from the study, and sharing of anonymized datasets. The experimental protocols were approved by the Ethics Committee of the National Institutes of Natural Sciences (Protocol Number: EC01-64). All experiments were conducted in accordance with the principles of the Declaration of Helsinki.

Apparatus

Auditory and visual stimuli were generated using MATLAB (MathWorks, Natick, MA) and Psychophysics Toolbox routines (16). Auditory stimuli were delivered to subjects through MR-compatible headphones (KM-201W3; KOBATEL, Yokohama, Japan). Visual stimuli were rear-projected onto a screen at the back of the MRI bore through an oblique mirror mounted on the head coil. Visual stimuli were presented using a high-speed projector system (PROPixx Lite, VPX-PRO-5000A; VPixx Technologies, Saint-Bruno, QC, Canada) with a spatial resolution of 1,920 pixels × 1,080 pixels and a refresh rate of 60 Hz. The distance from the eye to the screen was 141.3 cm, and the screen size was 32.3 cm × 18.2 cm (13.0° × 7.4° in visual angle).

Stimuli and Experimental Conditions

Auditory stimuli.

The auditory stimuli were two different tones of beep sounds (293 and 329 Hz) that switched unpredictably during 17-s stimulus blocks. During the stimulus blocks, auditory stimuli were presented for 800 ms, followed by a 200-ms silent (blank) period in each second. The auditory stimuli were presented to one ear.

Visual stimuli.

The visual stimuli were similar to those used in a previous study (17). The visual stimuli were a 120° sector of the annulus (inner radius: 2.1°; outer radius: 5.3°), equally divided into upper and lower parts by the horizontal meridian. The upper and lower parts of the stimulus were filled with a drifting square-wave grating (Fig. 1*A*; spatial frequency, 0.08 cycles per degree of polar angle; temporal frequency, 5 Hz; contrast, 90%) that continuously moved in opposite directions (clockwise or counterclockwise). The motion direction of the visual stimuli was reversed unpredictably during a 17-s stimulus block (see *Experimental conditions and procedure*). During the stimulus blocks, visual stimuli were presented for 800 ms, followed by a 200-ms blank period with a gray screen every second. The visual stimuli were presented on either the left or right side of the screen.

Experimental conditions and procedure.

We used a block-design paradigm for the fMRI experiment with auditory and visual stimulus presentation (Fig. 1*B*). In each run, either auditory or visual stimuli were presented, but never both simultaneously. Each run started with an initial 16-s rest block. The stimulus and rest blocks were alternately repeated. Each stimulus block of 17 s was followed by a rest block, which presented a uniform gray screen for 16 s (Fig. 1*B*). During 17-s stimulus blocks, the tone of the beep sounds (Fig. 1*C*), or the motion direction of the drifting grating (Fig. 1*D*), changed randomly every 1–3 s. Each run consisted of 10 repetitions of the stimulus and rest blocks. The total duration of each experimental run was 346 s.

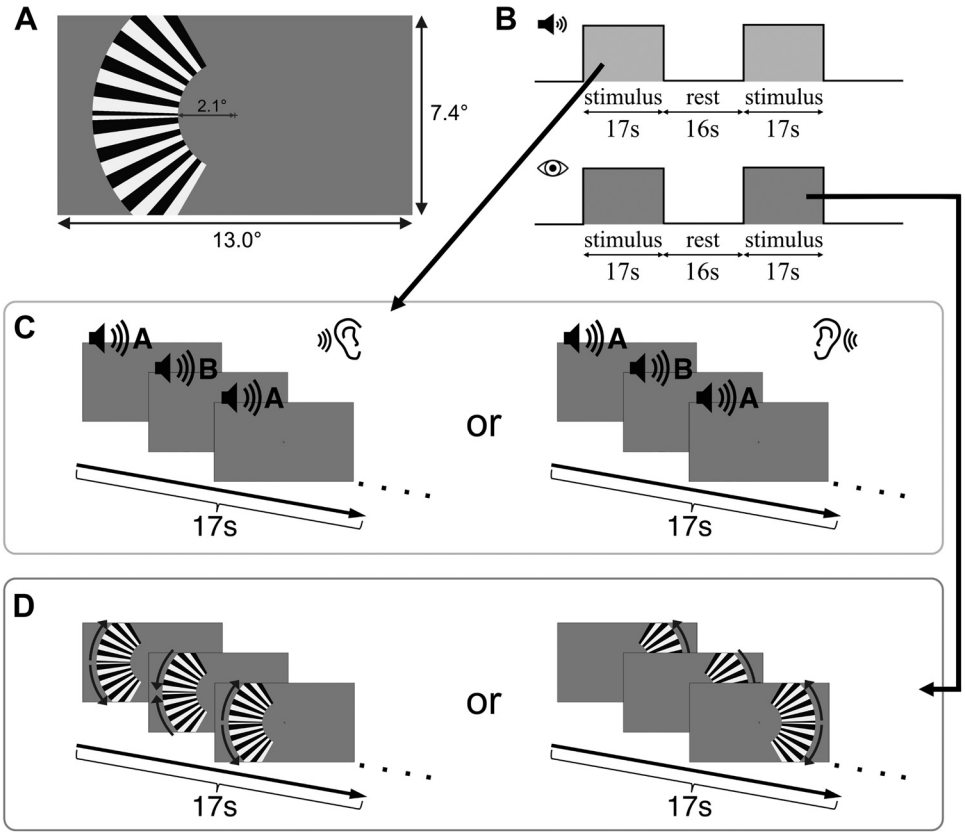

Figure 1. Stimulus and tasks. *A*: the visual stimuli (drifting gratings presented in the left or right visual field). The grating presented in the left visual field is shown as an example. The fixation cross was presented in the center of the screen. *B*: schematic figure of the stimulus and rest blocks. Auditory (*top*) or visual stimuli (*bottom*) were presented during the stimulus blocks for 17 s. Stimulus blocks were followed by rest blocks, in which the equiluminant background was displayed for 16 s. The stimulus and rest blocks were repeated 10 times in each run. *C*: schematic figure of a time series of auditory stimulus presentations in stimulus blocks. During stimulus blocks of 17 s, the tone of the beep sound switched randomly every 1–3 s. Subjects were asked to count the number of switches that occurred during the run. Stimuli were presented in the left or right ear during each block (examples are shown in the *left* and *right*, respectively). *D*: schematic figure of a time series of visual stimulus presentations in stimulus blocks. During stimulus blocks of 17 s, the direction of motion was randomly reversed every 1–3 s. Subjects were asked to count the number of reversals that occurred during the run. Stimuli were presented in either the left or right visual field during each block (examples are shown in the *left* and *right* panels, respectively).

Subjects underwent eight runs of fMRI experiment (four for the visual condition and four for the auditory condition). The auditory and visual runs were interleaved. Subjects were informed during breaks about which stimulus type would be presented in the next run.

Task.

Subjects were instructed to detect changes in the auditory or visual stimuli while keeping their eyes open and fixating on a black cross at the center of a projection screen. After each run, subjects verbally reported the number of changes to the experimenter. Although this task is demanding, subjects completed it with 97.1 ± 3.2% accuracy (means ± one standard deviation across subjects).

MRI Data Acquisition

Structural MRI data.

All subjects underwent the structural MRI data acquisition using a 3 T MRI scanner (MAGNETOM Verio; Siemens Healthcare GmbH, Erlangen, Germany) at the National Institute for Physiological Sciences with a 32-channel receiving head coil on a separate day from the 7 T fMRI experiment. We acquired the T1-weighted magnetization-prepared rapid gradient-echo (MP-RAGE) images [voxel size: 0.8 mm isotropic; repetition time (TR): 2,400 ms; echo time (TE): 2.24 ms; flip angle: 8°; inversion time: 1,060 ms] from all subjects. In addition, we acquired T2-weighted sampling perfection with application-optimized contrast using different flip angle evolution (SPACE) images (voxel size: 0.8 mm isotropic; TR: 3,200 ms; TE: 560 ms) from all subjects, as this image can be used as part of preprocessing (see *fMRI data preprocessing*).

We acquired structural images using 3 T MRI, because the image intensity of T1-weighted images is more homogeneous at 3 T owing to more uniform radiofrequency excitation and reduced dielectric effects, compared with 7 T MRI (18). In addition, the 3 T MRI provides higher-quality T2-weighted images, which are useful for correcting bias fields and identifying and removing veins and the dura mater, structures that are not clearly distinguishable from gray matter in T1-weighted images (19, 20). Therefore, we used structural data acquired with a 3 T scanner for surface-based localization of ROIs in individual subjects. Notably, recent studies using 7 T have adopted magnetization-prepared 2 rapid acquisition gradient echo (MP2RAGE) (21) to overcome the limitations of using 7 T structural data for tissue segmentation (22).

Functional MRI data.

The fMRI data were acquired using a 7 T MRI scanner (Magnetom 7 T; Siemens Healthcare GmbH, Erlangen, Germany) at the National Institute for Physiological Sciences with a 32-channel receiving head coil and a single-channel transmitting coil (Nova Medical Inc., Wilmington, MA). We used a multi-band, gradient-echo, echo-planar imaging (EPI) sequence provided by the Center for Magnetic Resonance Research, University of Minnesota (23) (https://www.cmrr.umn.edu/multiband/). Whole brain fMRI images were acquired with an isotropic voxel size of 1.6 mm [TR: 1,000 ms; TE: 22 ms; flip angle, 45°; field of view: 208 × 208 mm^2; multi-band acceleration factor: 5; generalized auto-calibrating partially parallel acquisition (GRAPPA)

acceleration factor: 2; bandwidth: 1,923 Hz/Px; echo spacing: 3.2 ms; phase-encoding direction: anterior-posterior (AP)].

In addition to the fMRI data, we acquired two spin-echo EPI datasets with reversed phase-encoding directions (anterior-posterior and posterior-anterior) before fMRI data acquisition. Three volumes of spin-echo EPI data were acquired using the same parameters (TR: 8,000 ms; TE: 60 ms; flip angle: 90°), resulting in the same geometric distortions as the fMRI data. We used these data for subsequent corrections of geometric distortions owing to susceptibility-induced artifacts (see *fMRI data preprocessing*).

MRI Data Analysis

fMRI data preprocessing.

We used a preprocessing pipeline for the fMRI data developed based on the Human Connectome Project (HCP) pipeline (19, 20). Particularly, we applied gradient nonlinearity, susceptibility-induced distortion, and motion correction. The preprocessed fMRI data were subsequently coregistered to the T1-weighted image acquired from the same subject using a 3 T MRI. The T2-weighted images were further used to separate the veins and dura mater from the gray matter. All preprocessing steps were performed in the native space of each subject to avoid loss of spatial resolution derived from normalization to the template brain (24, 25).

Identification of ROIs from structural MRI data.

We identified ROIs in the native space of each subject by analyzing the T1-weighted MRI data. We identified ROIs based solely on structural MRI data to avoid statistical circularity that can occur if the ROIs are identified from fMRI data.

Subcortical ROIs

We identified the MGN and LGN based on thalamic nuclei segmentation (26) on T1-weighted images. Briefly, this segmentation was performed based on a probabilistic atlas developed by combining ex vivo MRI and histology of the human thalamus (26). Examples of the MGN and LGN ROI identified in a representative subject are shown in Fig. 2*A*. Further details of this segmentation method are described in the original work (26) and are publicly available as part of FreeSurfer (27) (https://surfer.nmr.mgh.harvard.edu/fswiki/FreeSurferVersion3).

Primary Auditory Cortex ROI

We also identified the primary auditory cortex (A1) ROI based on the FreeSurfer cortical parcellation generated from T1-weighted images. We used two parcellation schemes implemented in FreeSurfer: the Desikan-Killiany (28) and Destrieux (29) atlases. Although the A1 is typically considered to correspond to Brodmann area 41, Brodmann area 42 is often also classified as a part of the A1 (30). Therefore, we merged one ROI (ctx-transversetemporal; lh: 1034; rh: 2034) in the Desikan-Killiany Atlas and one ROI (ctx_S_temporal_transverse; lh: 11175; rh: 12175) in the Destrieux Atlas to generate a single ROI that broadly covered the cortical areas defined as the A1 in the anatomical literature (31, 32) for each hemisphere. An example of the A1 ROI on the cortical surface of a representative subject is shown in Fig. 3*A*.

Visual Cortex ROIs

We identified the visual cortex ROIs (V1, V2, and V3) using the Benson atlas (33, 34) for T1-weighted images. Briefly, the Benson atlas is a template for a two-dimensional algebraic model of retinotopic maps (V1, V2, and V3) in the human brain derived from actual fMRI-based retinotopy measurements. Using a mass-spring-damper simulation, a method proposed by Benson et al. (34), we registered retinotopic templates to individual subjects' native space data. This method has been shown to accurately predict retinotopic representation based solely on structural MRI images (34). The pipeline for performing Benson atlas fitting is implemented as part of a publicly available neuropythy tool (https://github.com/noahbenson/neuropythy).

By fitting the Benson atlas to the individual subject's native space, we obtained the ROIs for V1, V2, and V3. We further subdivided these ROIs based on eccentricity to account for the fact that visual stimuli were only presented in restricted visual fields (see Fig. 1*A*) and to perform exploratory analysis to evaluate cross-modal NBR in relation to eccentricity representation. Specifically, each of V1, V2, and V3 was divided into four eccentricity-defined ROIs: foveal (Fov; 0°–2.1°), middle-peripheral (Mid; 2.1°–5.3°), peripheral (Peri; 5.3°–20°), and far-peripheral (Far; 20°–80°).

Resampling ROIs into fMRI Resolution

We resampled all ROIs identified in the aforementioned steps into a 1.6-mm isotropic voxel size to match the ROI and fMRI data resolution. In subsequent analyses, we used these resampled ROIs for ROI-based fMRI data analyses.

Evaluating the time course and activation evoked by sensory stimuli in ROIs.

To evaluate the BOLD responses evoked by sensory stimuli, we analyzed the time course of the BOLD responses in each ROI. We first averaged the fMRI data across all voxels belonging to the same ROI to obtain the average time course for each ROI.

The baseline was defined as the mean signal across five TRs preceding stimulus onset (−4, −3, −2, −1, and 0 s). The percent signal change at each time point was calculated using the following formula:

$$\%\ \text{signal change} = (\text{signal} - \text{baseline})/\text{baseline} \qquad (1)$$

We calculated the percent signal change separately for each stimulus block. The resulting time courses were averaged across blocks with identical stimulus conditions. These averaged time courses in each stimulus condition and ROI were subsequently used for visualization.

For statistical analysis, a single summary value was derived for each ROI, stimulus condition, and subject by averaging the percent signal change over 5–22 s after stimulus onset, considering the range of hemodynamic delays reported in block-design sensory fMRI studies (5–6 s; 35). The resulting values are visualized in violin plots (36) (https://zenodo.org/records/4559847).

We did not apply the hemodynamic response function (HRF) to estimate the response amplitudes of positive or negative BOLD responses because the BOLD time course in the visual cortex during the auditory condition exhibited an

atypical temporal profile that could not be accounted for by using canonical HRFs. Instead, we used a simple averaging of the time course to calculate the percent signal change, as it does not require any assumptions about the HRF.

Statistical analysis and visualization.

Statistical evaluation. We performed statistical tests on the percent signal change (averaged across time courses) in each ROI. First, we conducted a one-sample, two-tailed t test to assess whether the percent signal change in each ROI was significantly above or below the baseline. Second, we performed a two-tailed paired t test to evaluate whether the percent signal change in each ROI differed between the ipsilateral and contralateral hemispheres with respect to the stimulus presentation. We also quantified the effect size for this comparison by calculating Cohen's d. Third, we performed a one-way analysis of variance (ANOVA) to evaluate the statistical differences in the percent signal change across visual area ROIs with different eccentricity representations. In all tests, we defined the statistical significance threshold (α) as $P = 0.05$.

Visualization of percent signal change in each ROI. We visualized the distribution of percent signal changes across subjects using a violin plot (36) (https://zenodo.org/records/4559847).

Visualization of data on cortical surface. In addition to the primary statistical analysis performed in each ROI, we visualized a statistical map of auditory and visual conditions on the cortical surface using the 3dDeconvolve in AFNI (Analysis of Functional NeuroImages; https://afni.nimh.nih.gov/) (37, 38) and SUMA (39). Specifically, we performed a t test using 3dDeconvolve and visualized statistical maps on the cortical surface using SUMA with an uncorrected threshold of $P = 0.001$. Notably, this analysis was performed for descriptive visualization because evaluating the whole brain statistical contrast was not the primary interest of this study.

Evaluating the split-half reliability.

We evaluated the reliability of the cross-modal NBR in each condition and ROI by calculating the split-half reliability. To this end, we divided the fMRI data into odd and even blocks for each stimulus condition and separately calculated the percent signal change for each condition and ROI. We then calculated the inter-subject Pearson correlation of the percent signal change in each condition and ROI to assess the reliability of the cross-modal NBR. We also report the P value for each Pearson correlation as supplementary statistical information.

RESULTS

BOLD Responses in the MGN and LGN to Sensory Stimuli

We first examined the BOLD responses in the subcortical regions (MGN and LGN; Fig. 2*A*) evoked by auditory or visual stimuli to determine whether these regions exhibited cross-modal NBRs. Figure 2, *B* and *C* shows the percent signal changes in the MGN and LGN during the auditory and visual tasks. Data from the ROIs in the hemispheres ipsilateral and contralateral to stimulus presentation were analyzed separately.

BOLD responses in both the ipsilateral and contralateral MGN ROI were significantly higher than zero during the auditory blocks, suggesting the presence of a positive BOLD response evoked by auditory stimuli (Fig. 2*B*; one-sample two-tailed t test, ipsilateral: $t_{14} = 4.80$, $P < 0.001$; contralateral: $t_{14} = 6.97$, $P < 0.001$). Although both the ipsilateral and contralateral ROIs showed significant positive BOLD responses, the contralateral ROI exhibited a significantly higher percent signal change ($d = 0.83$; two-tailed paired t test, $t_{14} = 3.52$, $P = 0.003$). These results suggest that the auditory stimuli presented in the experiment successfully evoked the expected positive BOLD responses in the MGN. Although the positive BOLD response showed contralateral dominance, it was also evident in the ipsilateral ROI. In contrast to the visual system, the auditory system is not strictly lateralized to the contralateral ear, as suggested in the literature (40) and reported in previous fMRI studies (14, 41).

The contralateral LGN ROI showed BOLD responses significantly above zero during the visual blocks (Fig. 2*C*; $t_{14} = 4.06$, $P = 0.001$), replicating the results of previous fMRI studies (42, 43). In contrast, the ipsilateral LGN did not show significant BOLD responses (Fig. 2*C*; $t_{14} = 0.51$, $P = 0.62$). The contralateral LGN showed a significantly greater percent signal change than the ipsilateral LGN during visual blocks ($d = 0.69$, $t_{14} = 4.98$, $P < 0.001$). Taken together, these results indicate that visual stimuli reliably evoked the expected positive BOLD responses in the LGN, restricted to the contralateral side, consistent with the known anatomy of visual pathways.

After confirming the expected positive BOLD responses in both the auditory (MGN) and visual (LGN) thalamic ROIs, we examined their responses to stimuli from other sensory modalities to evaluate the cross-modal NBR in the subcortex. The MGN did not show BOLD responses significantly above or below zero during visual blocks in either hemisphere (Fig. 2*C*; ipsilateral: $t_{14} = -0.01$, $P = 0.99$; contralateral: $t_{14} = 1.09$, $P = 0.29$). Similarly, the LGN did not show BOLD responses significantly above or below zero during the auditory blocks in either hemisphere (Fig. 2*B*; ipsilateral: $t_{14} = 0.76$, $P = 0.46$; contralateral: $t_{14} = 1.39$, $P = 0.19$). These results indicate no significant evidence of cross-modal NBR in the MGN or LGN.

Positive BOLD Responses in the Primary Auditory and Primary Visual Cortex Evoked by Corresponding Sensory Stimuli

We evaluated the BOLD responses in the cortical ROIs (A1 and V1) evoked by sensory stimuli of the corresponding modalities. Figure 3*A* shows the percent signal change during the auditory blocks in the A1 (location of the ROI in a representative subject is shown in Fig. 3*A*, *top left*). The time course of the percent signal change in the contralateral hemisphere (Fig. 3*A*, *bottom left*) showed a positive BOLD response to auditory stimuli, following the hemodynamic delay. The percent signal change in the A1 during the auditory block was significantly above zero in both the ipsilateral and contralateral hemispheres (Fig. 3*A*, *bottom left* and *right*; ipsilateral: $t_{14} = 10.43$, $P < 0.001$; contralateral: $t_{14} = 14.25$, $P < 0.001$). The percent signal change in the contralateral A1 was significantly higher than that in the ipsilateral A1 ($d = 1.63$, $t_{14} = 16.28$, $P < 0.001$). These results indicate that auditory stimuli reliably evoked positive BOLD responses in A1,

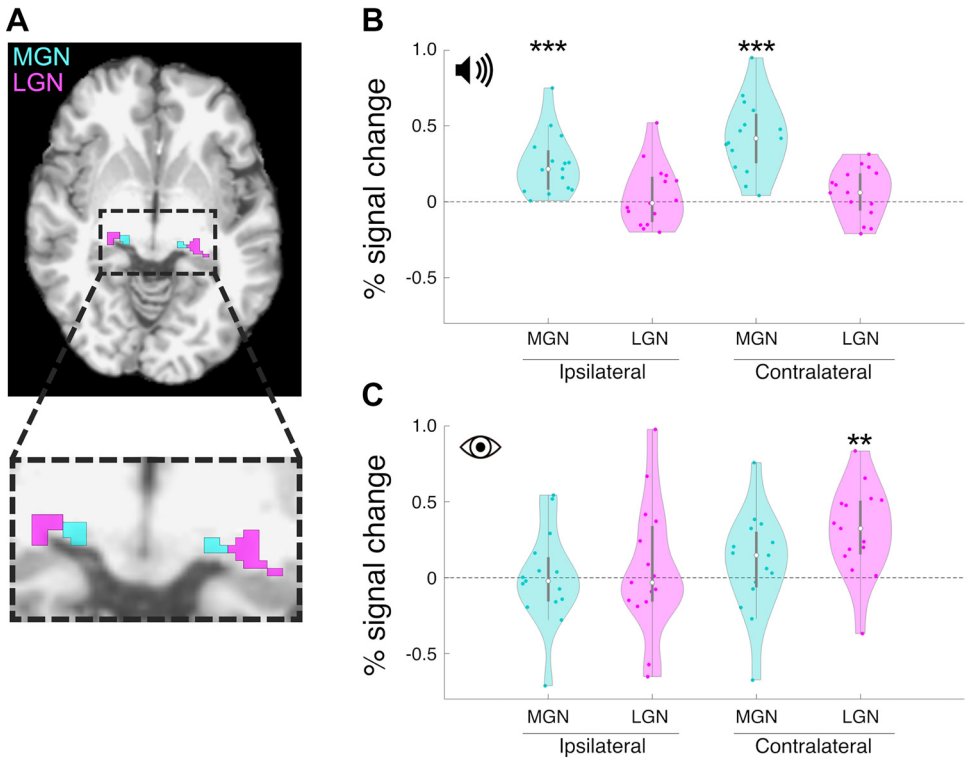

Figure 2. Results for subcortical regions of interest (ROIs). *A*: location of the medial geniculate nucleus (MGN; cyan) and lateral geniculate nucleus (LGN; magenta) overlaid on an axial slice of a T1-weighted image of a representative subject. The dotted rectangle depicts regions magnified in the bottom panel. *B*: blood oxygenation level-dependent (BOLD) response in MGN and LGN when auditory stimuli were presented to the ipsilateral or contralateral ears. The vertical axis represents the percent signal changes averaged across data from 5 to 22 s after stimulus onset. Each dot represents data from an individual subject. The white circle in each condition represents the median, whereas gray lines represent the first and third quartiles. Although MGN exhibited a positive BOLD response to auditory stimuli, no evidence of cross-modal negative BOLD response (NBR) was found in the LGN. The width of the shadowed area represents the approximate frequency of data points. *C*: BOLD response in the MGN and LGN when visual stimuli were presented to the ipsilateral or contralateral visual field. Although the LGN showed a positive BOLD response when stimuli were presented in the contralateral visual fields, we did not find a significant cross-modal NBR in the MGN. Asterisks indicate significant difference in the percent signal change from zero: $^{**}P < 0.01$, $^{***}P < 0.001$.

as expected. Similar to the MGN, auditory stimuli evoked bilateral positive BOLD responses with contralateral dominance in the response magnitude.

Figure 3*B* shows the percent signal change during the visual blocks in the V1 (location of the ROI in a representative subject is shown in Fig. 3*B*, *top*). The time course of the percent signal change in the contralateral hemisphere (Fig. 3*B*, *bottom left*) showed positive BOLD responses to visual stimuli in eccentricity ROIs corresponding to the stimulus position on the screen [Fov (0°–2.1°) and Mid (2.1°–5.3°)]. During visual blocks, percent signal change in the V1 Fov and Mid ROIs was significantly above zero in the contralateral hemisphere whereas Peri (5.3°–20°) and Far (20°–80°) ROIs were significantly below zero in both hemispheres (Fig. 3*B*, *bottom right*; contralateral Fov: $t_{14} = 2.17$, $P = 0.048$; contralateral Mid: $t_{14} = 6.21$, $P < 0.001$; contralateral Peri: $t_{14} = -2.69$, $P = 0.02$; contralateral Far: $t_{14} = -3.96$, $P = 0.001$; ipsilateral Peri: $t_{14} = -3.36$, $P = 0.005$; ipsilateral Far: $t_{14} = -3.38$, $P = 0.005$). The observed NBR in the ROIs representing eccentricity outside the stimulus or in the ipsilateral hemisphere was consistent with previous studies (44). The contralateral V1 showed significantly higher percent signal change than ipsilateral V1 in Fov and Mid ROIs (Fov; $d = 0.34$, $t_{14} = 3.36$, $P = 0.005$; Mid; $d = 1.26$, $t_{14} = 6.60$, $P < 0.001$), but significantly lower percent signal change in the Far ROI ($d = -0.17$, $t_{14} = -5.01$, $P = 0.001$). No significant difference was observed in the Peri ROI (Peri: $d = 0.14$, $t_{14} = 1.17$, $P = 0.26$).

The BOLD responses in V2 and V3 showed characteristics similar to those in V1 (Supplemental Fig. S1). Specifically, in the contralateral hemisphere, Fov and Mid ROI exhibited significant positive BOLD responses (V2: Fov: $t_{14} = 2.81$, $P = 0.014$; Mid: $t_{14} = 6.96$, $P < 0.001$; V3: Fov: $t_{14} = 6.09$, $P < 0.001$; Mid: $t_{14} = 14.13$, $P < 0.001$). In contrast, Peri and Far ROIs in V2 exhibited significant NBR (Peri: $t_{14} = -3.90$, $P = 0.002$; Far: $t_{14} = -7.07$, $P < 0.001$), and Far ROI in V3 exhibited significant NBR (Far: $t_{14} = -5.25$, $P < 0.001$). In the Mid ROI, the percent signal change was significantly greater in the contralateral than in the ipsilateral V2 and V3 (V2: $d = 1.41$, $t_{14} = 5.60$, $P < 0.001$; V3: $d = 1.78$, $t_{14} = 5.16$, $P < 0.001$).

These results indicate that the auditory and visual stimuli presented during the experiment evoked positive BOLD responses in the auditory and visual cortices, respectively, in the expected manner. Subsequent analyses focused on the cross-modal NBR in these cortical ROIs.

Cross-Modal NRBs in the Primary Auditory Cortex Are Observed Irrespective of the Stimulated Visual Field

We first evaluated the BOLD response in A1 under the visual condition. Figure 4*A* shows statistical maps of BOLD responses in A1 during the visual condition, mapped onto

the cortical surface of a representative subject (the location of the ROI on the whole brain surface is shown in Fig. 4*A*, *left*). We found that the NBR was evoked by visual stimuli in both hemispheres (Fig. 4*A*, *right*).

Figure 4*B* depicts the time course of the percent signal change in A1 in the hemispheres ipsilateral and contralateral to the stimulated visual field. The time courses were similar between the ipsilateral and contralateral hemispheres. The percent signal change was significantly below zero in both hemispheres (Fig. 4*C*; ipsilateral: $t_{14} = -3.19$, $P = 0.007$; contralateral: $t_{14} = -2.83$, $P = 0.01$), supporting the presence of a bilateral cross-modal NBR.

We then evaluated the reproducibility of the observed cross-modal NBR. We divided the fMRI data into odd and even blocks and calculated the split-half reliability of the percent signal change (Fig. 4*D*). We found significant inter-subject correlations between odd and even blocks in both hemispheres, supporting the high split-half reliability of the

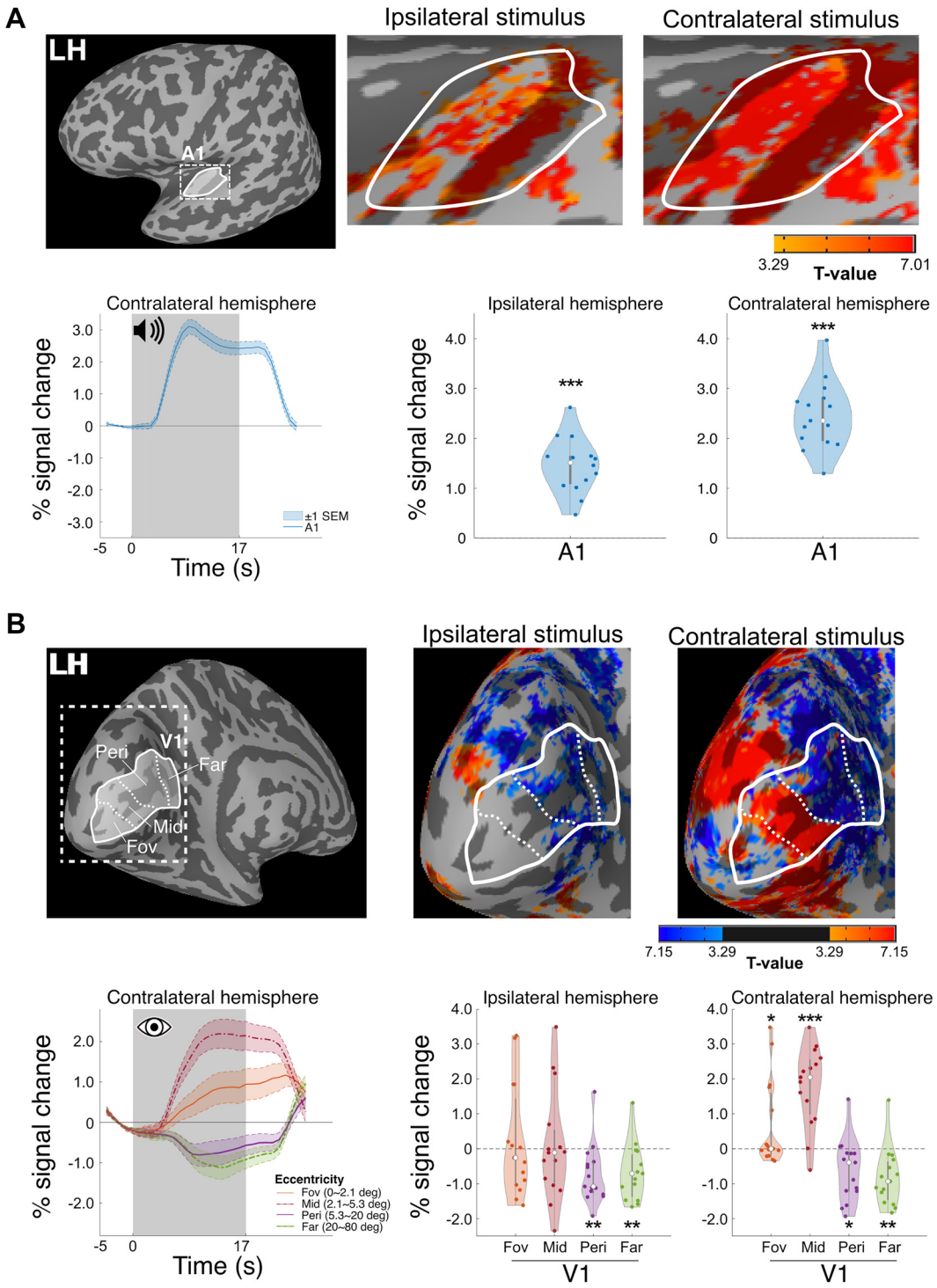

observed cross-modal NBR in A1 (ipsilateral: $r = 0.78$, $P = 0.001$; contralateral: $r = 0.74$, $P = 0.002$).

In summary, we observed that cross-modal NBR evoked by visual stimuli in the A1 was present in both hemispheres, irrespective of the visual field stimulated by the stimuli, suggesting that cross-modal NBR in the auditory cortex is not a mere epiphenomenon of positive BOLD responses in the visual cortex.

BOLD Responses in the Visual Cortex to Auditory Stimuli

Finally, we evaluated BOLD responses in the visual cortex under the auditory condition. Figure 5*A* shows the statistical maps of BOLD responses in the visual cortex during the auditory condition on the cortical surface of a representative subject, with ROIs displayed in the *left*. The presence of cross-modal NBR in the visual cortex was not observed in all subjects, although the data shown in Fig. 5*A* indicate some presence of NBR in this subject. Because the time course of the percent signal change was similar between hemispheres, ipsilateral and contralateral to the stimulated ear, across all visual cortex ROIs (Supplemental Fig. S2), subsequent analyses were performed on data averaged across both hemispheres.

Figure 5*B* (*left*) depicts the time course of the percent signal change during the auditory condition in V1, V2, and V3. The averaged hemodynamic response across subjects was atypical, showing no sustained positive or negative BOLD response despite the block-design presentation of auditory stimuli. This atypical pattern likely reflects a large inter-subject variability in the BOLD response (see Supplemental Fig. S3 for individual time courses). Figure 5*B* (*right*) shows the percent signal change in each ROI. In all cases, we found considerable individual variation in the BOLD responses. Due to this variability, no ROI exhibited percent signal change significantly above or below zero (V1 Fov: $t_{14} = -0.24$, $P = 0.81$; V1 Mid: $t_{14} = -0.29$, $P = 0.78$; V1 Peri: $t_{14} = -0.04$, $P = 0.97$; V1 Far: $t_{14} = -1.01$, $P = 0.33$; V2 Fov: $t_{14} = 0.47$, $P = 0.64$; V2 Mid: $t_{14} = -0.43$, $P = 0.68$; V2 Peri: $t_{14} = -0.95$, $P = 0.36$; V2 Far: $t_{14} = -1.52$, $P = 0.15$; V3 Fov: $t_{14} = 0.88$, $P = 0.39$; V3 Mid: $t_{14} = -0.06$, $P = 0.95$; V3 Peri: $t_{14} = -1.28$, $P = 0.22$; V3 Far: $t_{14} = -1.51$, $P = 0.15$). These results suggest that there is no statistical support for the cross-modal NBR at the population level. In addition, we found no significant main effect of eccentricity in the one-way ANOVA for the percent signal change in V1, V2, and V3 (V1, $F_{3,56} = 0.14$, $P = 0.93$; V2, $F_{3,56} = 0.82$, $P = 0.49$; V3, $F_{3,56} = 1.35$, $P = 0.27$).

We assessed the split-half reliability of the percent signal change during the auditory condition in the visual cortical ROIs (Fig. 5*C*). We found significant correlations between odd and even blocks in all eccentricity ROIs in V1, V2 and V3 (V1: Fov, $r = 0.82$, $P < 0.001$, Mid, $r = 0.77$, $P = 0.001$, Peri, $r = 0.78$, $P < 0.001$, Far, $r = 0.88$, $P < 0.001$; V2: Fov, $r = 0.80$, $P < 0.001$, Mid, $r = 0.65$, $P = 0.009$, Peri, $r = 0.66$, $P = 0.007$, Far, $r = 0.77$, $P < 0.001$; V3: Fov, $r = 0.78$, $P < 0.001$, Mid, $r = 0.69$, $P = 0.004$, Peri, $r = 0.75$, $P = 0.001$, Far, $r = 0.84$, $P < 0.001$). These results suggest that large individual variations may reflect reproducible individual differences, rather than measurement noise or limited data quality.

Taken together, we found that the cross-modal NBR in the visual cortex was present in some subjects but not in others. This large individual difference was consistent between odd and even blocks.

DISCUSSION

We evaluated the cross-modal NBR in human subcortical and cortical regions by analyzing 7 T fMRI data during auditory and visual conditions. We did not find evidence of cross-modal NBR in the subcortical ROIs (MGN and LGN; Fig. 2). In contrast, in A1, we found a significant cross-modal NBR during the visual condition (Fig. 4). Importantly, we observed cross-modal NBR in both the ipsilateral and contralateral hemispheres with respect to visual stimulation. Finally, we found that the BOLD responses in the visual cortex during the auditory condition exhibited large individual differences, resulting in a lack of statistical evidence for cross-modal NBR at the group level (Fig. 5).

No Statistical Evidence of Cross-Modal NBR in the Subcortex

We did not find any significant evidence of cross-modal NBR in the MGN or the LGN (Fig. 2). These results are unlikely to be explained by mislocalization between the ROIs and fMRI data, as we observed clear positive BOLD responses in these ROIs evoked by stimuli of the corresponding sensory modality.

Physiological studies on macaques and rodents have demonstrated the existence of inhibitory input to the MGN and LGN from other subcortical nuclei, such as the thalamic reticular nucleus, as well as evidence of neural response inhibition when a stimulus in a different sensory modality is

Figure 3. Positive blood oxygenation level-dependent (BOLD) evoked by sensory stimuli is confirmed in the early auditory and visual cortex. *A*: positive BOLD response to auditory stimuli in the primary auditory cortex (A1) of a representative subject. *Top*: the location of the A1 region of interest (ROI) is shown by a white contour on the cortical surface (*left*). The dotted rectangle depicts regions magnified in the *middle* and *right*. Colored areas in the *middle* and *right* represent the *t* value of positive BOLD responses to auditory stimuli in the A1 ROI of each hemisphere. *Bottom left*: The time course of the BOLD response in the A1 when auditory stimuli were presented to the ears contralateral to ROIs. The vertical axis represents the percent signal change. The horizontal axis represents the time from stimulus onset (0 represents stimulus onset time, whereas the gray shaded area represents the stimulus block). The thick blue line represents the percent signal change averaged across all subjects, whereas the shadowed area represents ±1 SE across subjects. *Bottom middle and right*: violin plots of the percent signal change when auditory stimuli were presented to the ears ipsilateral or contralateral to the ROI (*middle* and *right*, respectively). *B*: positive BOLD response to visual stimuli in the primary visual cortex (V1) of a representative subject. *Upper*: the location of the V1 ROI is shown by a white contour on the cortical surface (*left*). The borders between V1 ROIs determined based on eccentricity (Fov, 0–2.1°; Mid, 2.1–5.3°; Peri, 5.3–20°; Far, 20–80°) are shown by white dotted lines. Colored areas in the *middle* and *right* depict the *t* values of positive (red) and negative BOLD responses (blue) to visual stimuli in the V1 ROI of each hemisphere (*middle*, ipsilateral; *right*, contralateral). *Bottom left*: The time course of the BOLD response in the V1 when visual stimuli were presented in the visual field contralateral to the ROI. Colored curves represent the course in each ROI (orange, Fov; red, Mid; purple, Peri; green, Far). Positive BOLD responses were observed in ROIs corresponding to the eccentricity of the visual stimulus. *Bottom middle and right:* violin plots of the percent signal change when visual stimuli were presented to visual fields ipsilateral (*middle*) or contralateral to the ROI (*right*). Conventions used in violin plots are identical to those used in Fig. 2, *B* and *C*. Asterisks indicate significant difference in the percent signal change from zero: $*P < 0.05$, $**P < 0.01$, $***P < 0.001$.

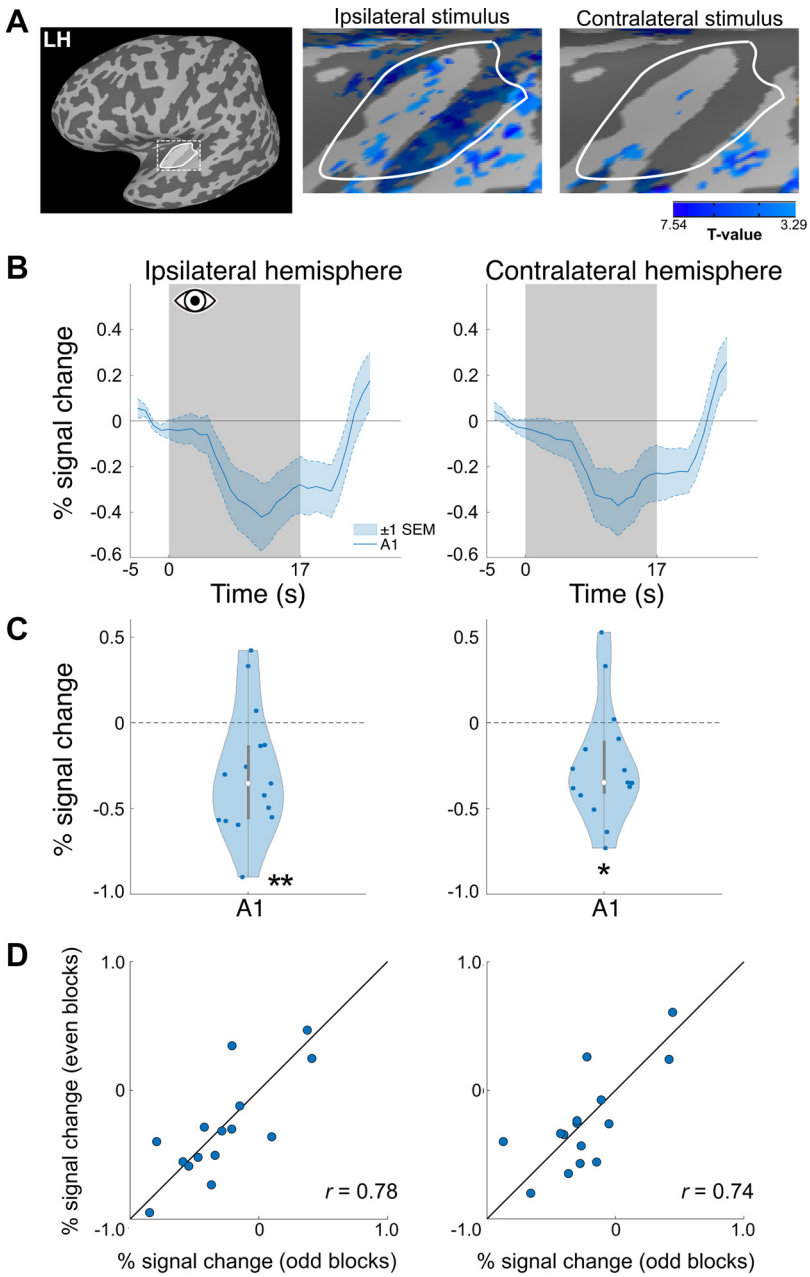

Figure 4. Cross-modal negative blood oxygenation level-dependent (BOLD) responses in the auditory cortex (A1). *A*, *left*: the location of the primary auditory cortex (A1) region of interest (ROI) (left hemisphere) is shown by a white contour on the cortical surface of a representative subject. The dotted rectangle depicts regions magnified in the right panel. *Middle* and *right*: the cross-modal negative BOLD response (NBR) to visual stimuli in the A1 ROI. Colored (blue) regions depict the *t* value of negative BOLD responses to visual stimuli in the A1 ROI of each hemisphere (*middle*, ipsilateral; *right*, contralateral). *B*: time course of the BOLD response in the ipsilateral and contralateral A1. *C*: the violin plot of the percent signal change in the ipsilateral and contralateral hemispheres. Cross-modal negative BOLD was similar between the ipsilateral and contralateral hemispheres. Asterisks indicate statistically significant difference in the percent signal change from zero: $*P < 0.05$, $**P < 0.01$. *D*: reproducibility of BOLD response to the visual stimuli in the A1. Each dot represents data from each subject, with the horizontal axis showing the mean percent signal change in odd blocks and the vertical axis showing that in even blocks. Split-half reliability (Pearson correlation between the odd and even blocks) was high in both the ipsilateral and contralateral hemispheres.

presented (45–47; see Ref. 48 for a review on the LGN). Given these findings, it is plausible that cross-modal suppression occurs in the human MGN and LGN. Although speculative, we have several hypotheses as to why we did not find support for cross-modal NBR in the MGN and LGN. First, cross-modal NBR may be present in the human subcortex with a smaller amplitude, but we may have failed to identify it due to the limited signal-to-noise ratio. However, given the robust cross-modal NBR in A1 (Fig. 4), any subcortical cross-modal NBR, if present, may be comparatively weaker. Second, considering the complex nature of NBR, BOLD responses receive different effects from inhibitory inputs compared with electrophysiological measurements (49, 50). If this is the case, cross-modal suppression may be more readily detectable using electrophysiological measurements in humans, such as intracranial electroencephalography. Third, the MGN and LGN have complex anatomical circuitry with respect to other brain regions, with both excitatory and inhibitory connections. For example, the LGN receives inputs from the pedunculopontine tegmental nucleus (51), which regulates the capacity of the LGN to process incoming sensory information for task execution (52, 53). The BOLD response may also be influenced by task-related signals, potentially masking cross-modal NBR. Resolving these hypotheses will require further investigation using improved fMRI techniques with higher signal specificity or by combining fMRI and electrophysiological measurements.

Presence of Cross-Modal NBR in the Auditory Cortex Irrespective of Stimulated Visual Fields

In A1, we found a significant cross-modal NBR in both hemispheres regardless of the stimulated visual field (Fig. 4*A*). In

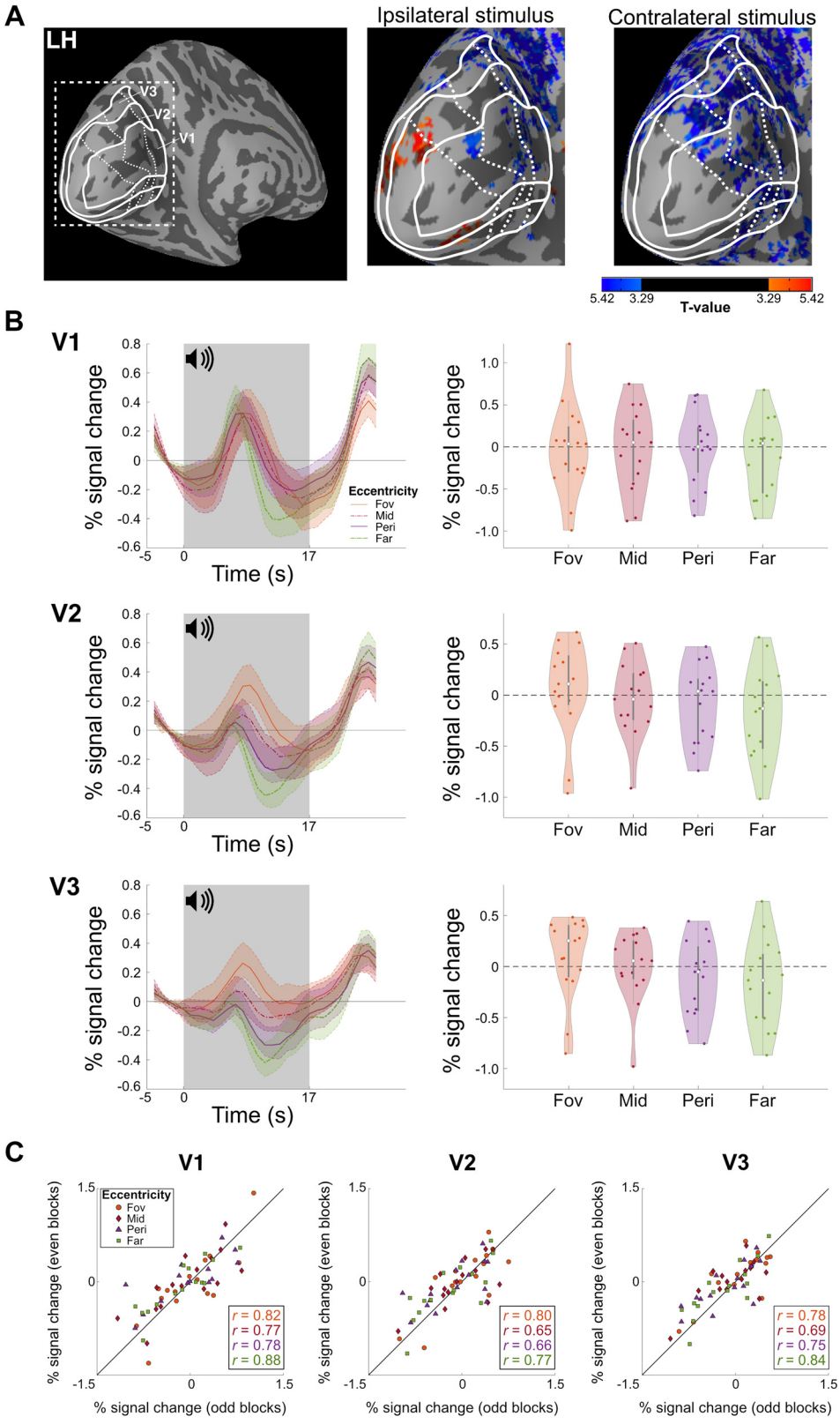

Figure 5. Cross-modal blood oxygenation level-dependent (BOLD) responses to the auditory stimuli in the visual cortex (V1, V2, and V3). *A*: surface view of the visual cortex in the left hemisphere of a representative subject. *Left*: a white contour on the cortical surface indicates the locations of the V1, V2, and V3 ROIs. The borders between regions of interest (ROIs) determined based on eccentricity (Fov, 0–2.1°; Mid, 2.1–5.3°; Peri, 5.3–20°; Far, 20–80°) are shown by white dotted lines. The dotted rectangle depicts regions magnified in the *right*. *Middle* and *right*: BOLD responses to auditory stimuli in visual ROIs. The colored areas depict the *t* values of positive (red) and negative BOLD responses (blue) to auditory stimuli in the V1, V2, and V3 ROIs of each hemisphere (*middle*, ipsilateral; *right*, contralateral). *B*, *left:* time course of the BOLD response in V1 (*top*), V2 (*middle*), and V3 (*bottom*). *Right*: violin plot of the percent signal change. Both time courses and violin plots represent the average across the two hemispheres. *C*: reproducibility of cross-modal BOLD responses to the auditory stimuli in the visual cortex (*left*, V1; *middle*, V2; *right*, V3). Each dot represents data from each subject, with the colors indicating the eccentricity-based ROIs. The horizontal axis shows the mean percent signal change in odd blocks, and the vertical axis shows that in even blocks. The split-half reliability was calculated using Pearson's correlation coefficient.

addition, the time courses of BOLD responses were similar between the hemispheres, ipsilateral and contralateral to the stimulated visual field. This result indicates that the cross-modal NBR in A1 is not an epiphenomenon of the positive BOLD response in the visual cortex, which is predominant in the hemisphere contralateral to the stimulated visual field (Fig. 3*B*). Therefore, the cross-modal NBR is more likely to reflect interhemispheric suppression, rather than mechanisms coordinated within the hemisphere. This result is consistent with a recent fMRI study (14) that reported a cross-modal NBR in the bilateral auditory cortex, despite visual stimulation being restricted to the right visual field.

Notably, previous studies have discussed the possibility that NBR can be explained by the blood-stealing effect, in which increased blood flow to one brain region can reduce blood flow to other areas, leading to NBR without direct neural suppression (50, 54–56). However, this hypothesis was originally proposed to explain the NBR in visual cortex regions representing the nonstimulated visual field, which lie adjacent to regions showing positive BOLD responses (50, 57). Given the large spatial distance between the auditory and visual cortices, the blood-stealing effect is unlikely to account for the cross-modal NBR observed in A1. Furthermore, because the left and right hemispheres have largely independent blood supplies, as discussed by Smith et al. (49), our results suggest that the cross-modal NBR in A1 is more plausibly driven by the suppression of neural activity than by blood-stealing, at least in the auditory cortex.

The idea that the cross-modal NBR in the auditory cortex may reflect neural suppression rather than blood-stealing is also consistent with observation from a previous animal study (58). In this study, the response of the auditory cortex of the guinea pig brain to visual stimuli was measured using optical imaging with a voltage-sensitive dye that reflects changes in the membrane potential. The authors found that the auditory cortex exhibited suppression of neural activity during visual stimulation, consistent with the idea that cross-modal suppression can be observed electrophysiologically in the auditory cortex.

BOLD Responses in the Visual Cortex during the Auditory Condition

We did not find a significant cross-modal NBR in the visual cortex because, unlike the auditory cortex, the time course as well as the percent signal change of the BOLD response was inconsistent across subjects (Fig. 5). Since the BOLD response exhibited considerable split-half reproducibility across subjects, these results may reflect genuine individual differences, with only some subjects showing robust cross-modal NBR in the visual cortex.

Although reproducible, this individual variability requires caution when interpreting its functional relevance. For example, these individual differences may reflect individual variability in hemodynamic responses rather than representing meaningful individual differences at the neuronal level. If this is the case, the observed individual differences may reflect vascular characteristics in the visual cortex rather than differences in neural information processing. Moreover, although the subjects were instructed to maintain fixation during the auditory condition, individual differences in microsaccades and blink frequency, both of which affect BOLD responses in the visual cortex (59), may also explain the observed variability. Therefore, the extent to which the individual variability of the cross-modal NBR in the visual cortex reflects differences in auditory-driven suppression of visual processing must be carefully examined in future studies, considering these confounding factors. Nonetheless, a rodent study supported the relationship between neural suppression in the visual cortex caused by auditory stimuli and behavior (60).

Limitations and Future Directions

Our study has several limitations. First, our 7 T MRI setup has a size restriction for the visual stimulus presentation owing to the head coil setup, resulting in a relatively narrow range of eccentricity that can be stimulated. This may have restricted both the size of the activated cortical regions and the magnitude of the evoked BOLD responses. However, we observed a robust cross-modal NBR in the auditory cortex (Fig. 4), suggesting that even stimulation limited to relatively foveal visual fields can be sufficient to evoke cross-modal NBR. Second, although we used a stimulus typically used for sensory fMRI experiments (5, 17), we could not test all types of stimuli owing to constraints on the scan time for human subjects. Although our auditory stimuli elicited a clear positive BOLD response in A1 (Fig. 3*A*), different types of auditory stimuli may evoke a more robust cross-modal NBR in the visual cortex. Third, we only tested conventional BOLD measurements with a relatively coarse voxel size (1.6 mm) to achieve a higher signal-to-noise ratio. Future studies using pulse sequences with greater specificity to local signals and measurements with higher spatial resolution may offer deeper insights into the laminar profiles of cross-modal NBR in the auditory and visual cortices (61–63).

Finally, because our study focused on healthy adults, the current observations may not be generalizable to other populations, such as children and older adults. Previous studies have demonstrated that the amplitudes of cross-modal NBR differ across age groups (13). In addition, cross-modal BOLD responses are expected to differ substantially in clinical populations, as previous studies have demonstrated that the visual cortex exhibits a positive response to auditory and tactile stimuli in patients with macular degeneration or blindness (3, 5). Therefore, a direct comparison between healthy and clinical populations with visual or auditory disorders would clarify how cross-modal BOLD responses depend on the presence of bottom-up sensory input.

Conclusions

In conclusion, we found a significant cross-modal NBR in the bilateral auditory cortex, regardless of the stimulated visual field. These results suggest that the cross-modal NBR in the auditory cortex is not a simple epiphenomenon of the positive BOLD response in the visual cortex of the hemisphere contralateral to the visual stimuli. However, we did not observe a significant cross-modal NBR in the sensory subcortex and visual cortex. The lack of group-level statistical evidence for cross-modal NBR in the visual cortex can be explained by large individual differences. These results suggest that the cross-modal NBR in the auditory cortex may more likely reflect an interhemispheric suppression mechanism rather than suppression coordinated within the same hemisphere.

DATA AVAILABILITY

The anonymized data required for replicating figures and statistical analysis are publicly available in the public repository (https://github.com/OkazakiTakemuraLab/CrossmodalNBRfMRI).

SUPPLEMENTAL MATERIAL

Supplemental Figs. S1–S3: https://doi.org/10.5281/zenodo.16072854.

ACKNOWLEDGMENTS

The authors thank Dr. Hans-Peter Fautz, Dr. Tobias Kober, Dr. Tim DeVito, Dr. Josef Pfeuffer, Saurabh Shah, Andreas Greiser, and Thomas Banner (Siemens Healthineers GmbH) for providing the sequences of prescanning adjustment on 7 T MRI. The authors also thank Kumiko Kobayashi for support of subject recruitment. The authors thank Editage (http://www.editage.com) for editing and reviewing the manuscript for the English language.

GRANTS

The Japan Society for the Promotion of Science (JSPS) KAKENHI under Grant/Award Number: JP23K20014 (to T. Miyata); JP21H03789 and JP24K03240 (to H.T.) and The MEXT Promotion of Development of a Joint Usage/Research System Project: Coalition of Universities of Research Excellence Program (CURE) under Grant/Award Number JPMXP1323015488.

DISCLOSURES

No conflicts of interest, financial or otherwise, are declared by the authors.

AUTHOR CONTRIBUTIONS

T. Miyata, T. Morita, and H.T. conceived and designed research; T. Miyata, M.F., J.L., I.Y., A.Y., and H.T. performed experiments; T. Miyata, T.Y., and J.Y. analyzed data; T. Miyata and H.T. interpreted results of experiments; T. Miyata prepared figures; T. Miyata, J.L., I.Y., T.Y., T. Morita, and H.T. drafted manuscript; T. Miyata, M.F., J.L., I.Y., T.Y., A.Y., J.Y., T. Morita, and H.T. edited and revised manuscript; T. Miyata, M.F., J.L., I.Y., T.Y., A.Y., J.Y., T. Morita, and H.T. approved final version of manuscript.

REFERENCES

1. **Burr D**, **Alais D.** Combining visual and auditory information. *Prog Brain Res* 155: 243–258, 2006. doi:10.1016/S0079-6123(06)55014-9.
2. **Angelaki DE**, **Gu Y**, **DeAngelis GC.** Multisensory integration: psychophysics, neurophysiology, and computation. *Curr Opin Neurobiol* 19: 452–458, 2009. doi:10.1016/j.conb.2009.06.008.
3. **Sadato N**, **Pascual-Leone A**, **Grafman J**, **Ibañez V**, **Deiber MP**, **Dold G**, **Hallett M.** Activation of the primary visual cortex by Braille reading in blind subjects. *Nature* 380: 526–528, 1996. doi:10.1038/380526a0.
4. **Striem-Amit E**, **Amedi A.** Visual cortex extrastriate body-selective area activation in congenitally blind people "seeing" by using sounds. *Curr Biol* 24: 687–692, 2014. doi:10.1016/j.cub.2014.02.010.
5. **Masuda Y**, **Takemura H**, **Terao M**, **Miyazaki A**, **Ogawa S**, **Horiguchi H**, **Nakadomari S**, **Matsumoto K**, **Nakano T**, **Wandell BA**, **Amano K.** V1 projection zone signals in human macular degeneration depend on task despite absence of visual stimulus. *Curr Biol* 31: 406–412.e3, 2021. doi:10.1016/j.cub.2020.10.034.
6. **Ogawa S**, **Tank DW**, **Menon R**, **Ellermann JM**, **Kim SG**, **Merkle H**, **Ugurbil K.** Intrinsic signal changes accompanying sensory stimulation: functional brain mapping with magnetic resonance imaging. *Proc Natl Acad Sci USA* 89: 5951–5955, 1992. doi:10.1073/pnas.89.13.5951.
7. **Kwong KK**, **Belliveau JW**, **Chesler DA**, **Goldberg IE**, **Weisskoff RM**, **Poncelet BP**, **Kennedy DN**, **Hoppel BE**, **Cohen MS**, **Turner R.** Dynamic magnetic resonance imaging of human brain activity during primary sensory stimulation. *Proc Natl Acad Sci USA* 89: 5675–5679, 1992. doi:10.1073/pnas.89.12.5675.
8. **Engel S**, **Zhang X**, **Wandell B.** Colour tuning in human visual cortex measured with functional magnetic resonance imaging. *Nature* 388: 68–71, 1997. doi:10.1038/40398.
9. **Binder JR**, **Rao SM**, **Hammeke TA**, **Yetkin FZ**, **Jesmanowicz A**, **Bandettini PA**, **Wong EC**, **Estkowski LD**, **Goldstein MD**, **Haughton VM.** Functional magnetic resonance imaging of human auditory cortex. *Ann Neurol* 35: 662–672, 1994. doi:10.1002/ana.410350606.
10. **Jäncke L**, **Loose R**, **Lutz K**, **Specht K**, **Shah NJ.** Cortical activations during paced finger-tapping applying visual and auditory pacing stimuli. *Brain Res Cogn Brain Res* 10: 51–66, 2000. doi:10.1016/s0926-6410(00)00022-7.
11. **Laurienti PJ**, **Burdette JH**, **Wallace MT**, **Yen YF**, **Field AS**, **Stein BE.** Deactivation of sensory-specific cortex by cross-modal stimuli. *J Cogn Neurosci* 14: 420–429, 2002. doi:10.1162/089892902317361930.
12. **Mozolic JL**, **Joyner D**, **Hugenschmidt CE**, **Peiffer AM**, **Kraft RA**, **Maldjian JA**, **Laurienti PJ.** Cross-modal deactivations during modality-specific selective attention. *BMC Neurol* 8: 35, 2008. doi:10.1186/1471-2377-8-35.
13. **Morita T**, **Asada M**, **Naito E.** Developmental changes in task-induced brain deactivation in humans revealed by a motor task. *Dev Neurobiol* 79: 536–558, 2019. doi:10.1002/dneu.22701.
14. **Nelson W**, **Mayhew SD.** Investigating the consistency of negative BOLD responses to combinations of visual, auditory, and somatosensory stimuli and their modulation by the level of task demand. *Hum Brain Mapp* 46: e70177, 2025. doi:10.1002/hbm.70177.
15. **Stewart EEM**, **Valsecchi M**, **Schütz AC.** A review of interactions between peripheral and foveal vision. *J Vis* 20: 2, 2020. doi:10.1167/jov.20.12.2.
16. **Brainard DH.** The Psychophysics Toolbox. *Spat Vis* 10: 433–436, 1997.
17. **Gouws AD**, **Alvarez I**, **Watson DM**, **Uesaki M**, **Rodgers J**, **Morland AB.** On the role of suppression in spatial attention: evidence from negative BOLD in human subcortical and cortical structures. *J Neurosci* 34: 10347–10360, 2014 [Erratum in *J Neurosci* 34: 14164, 2014]. doi:10.1523/JNEUROSCI.0164-14.2014.
18. **Allen EJ**, **St-Yves G**, **Wu Y**, **Breedlove JL**, **Prince JS**, **Dowdle LT**, **Nau M**, **Caron B**, **Pestilli F**, **Charest I**, **Hutchinson JB**, **Naselaris T**, **Kay K.** A massive 7T fMRI dataset to bridge cognitive neuroscience and artificial intelligence. *Nat Neurosci* 25: 116–126, 2022. doi:10.1038/s41593-021-00962-x.
19. **Glasser MF**, **Sotiropoulos SN**, **Wilson JA**, **Coalson TS**, **Fischl B**, **Andersson JL**, **Xu J**, **Jbabdi S**, **Webster M**, **Polimeni JR**, **Van Essen DC**, **Jenkinson M**; **WU-Minn HCP Consortium.** The minimal preprocessing pipelines for the Human Connectome Project. *Neuroimage* 80: 105–124, 2013. doi:10.1016/j.neuroimage.2013.04.127.
20. **Yamamoto T**, **Fukunaga M**, **Sugawara SK**, **Hamano YH**, **Sadato N.** Quantitative evaluations of geometrical distortion corrections in cortical surface-based analysis of high-resolution functional MRI data at 7T. *J Magn Reson Imaging* 53: 1220–1234, 2021. doi:10.1002/jmri.27420.
21. **Marques JP**, **Kober T**, **Krueger G**, **van der Zwaag W**, **Van de Moortele PF**, **Gruetter R.** MP2RAGE, a self bias-field corrected sequence for improved segmentation and T1-mapping at high field. *Neuroimage* 49: 1271–1281, 2010. doi:10.1016/j.neuroimage.2009.10.002.
22. **Mueller SG.** 7T MP2RAGE for cortical myelin segmentation: impact of aging. *PLoS One* 19: e0299670, 2024. doi:10.1371/journal.pone.0299670.
23. **Moeller S**, **Yacoub E**, **Olman CA**, **Auerbach E**, **Strupp J**, **Harel N**, **Uğurbil K.** Multiband multislice GE-EPI at 7 tesla, with 16-fold acceleration using partial parallel imaging with application to high spatial and temporal whole-brain fMRI. *Magn Reson Med* 63: 1144–1153, 2010. doi:10.1002/mrm.22361.
24. **Weiner KS**, **Grill-Spector K.** Neural representations of faces and limbs neighbor in human high-level visual cortex: evidence for a new organization principle. *Psychol Res* 77: 74–97, 2013. doi:10.1007/s00426-011-0392-x.

25. **Stelzer J**, **Lohmann G**, **Mueller K**, **Buschmann T**, **Turner R.** Deficient approaches to human neuroimaging. *Front Hum Neurosci* 8: 462, 2014. doi:10.3389/fnhum.2014.00462.
26. **Iglesias JE**, **Insausti R**, **Lerma-Usabiaga G**, **Bocchetta M**, **Van Leemput K**, **Greve DN**, **van der Kouwe A**, **Fischl B**, **Caballero-Gaudes C**, **Paz-Alonso PM**; **Alzheimer's Disease Neuroimaging Initiative.** A probabilistic atlas of the human thalamic nuclei combining ex vivo MRI and histology. *Neuroimage* 183: 314–326, 2018. doi:10.1016/j.neuroimage.2018.08.012.
27. **Fischl B**, **Salat D**, **Busa E**, **Albert M**, **Dieterich M**, **Haselgrove C**, **Kouwe A**, **Killiany R**, **Kennedy D**, **Klaveness S**, **Montillo A**, **Makris N**, **Rosen B**, **Dale A.** Whole brain segmentation automated labeling of neuroanatomical structures in the human brain. *Neuron* 33: 341–355, 2002. doi:10.1016/s0896-6273(02)00569-x.
28. **Desikan RS**, **Ségonne F**, **Fischl B**, **Quinn BT**, **Dickerson BC**, **Blacker D**, **Buckner RL**, **Dale AM**, **Maguire RP**, **Hyman BT**, **Albert MS**, **Killiany RJ.** An automated labeling system for subdividing the human cerebral cortex on MRI scans into gyral based regions of interest. *Neuroimage* 31: 968–980, 2006. doi:10.1016/j.neuroimage.2006.01.021.
29. **Destrieux C**, **Fischl B**, **Dale A**, **Halgren E.** Automatic parcellation of human cortical gyri and sulci using standard anatomical nomenclature. *Neuroimage* 53: 1–15, 2010. doi:10.1016/j.neuroimage.2010.06.010.
30. **Brodmann K.** *Vergleichende Lokalisationslehre der Grosshirnrinde in ihren Prinzipien dargestellt auf Grund des Zellenbaues*. Leipzig, 1909.
31. **Rademacher J**, **Morosan P**, **Schormann T**, **Schleicher A**, **Werner C**, **Freund HJ**, **Zilles K.** Probabilistic mapping and volume measurement of human primary auditory cortex. *Neuroimage* 13: 669–683, 2001. doi:10.1006/nimg.2000.0714.
32. **Fullerton BC**, **Pandya DN.** Architectonic analysis of the auditory-related areas of the superior temporal region in human brain. *J Comp Neurol* 504: 470–498, 2007. doi:10.1002/cne.21432.
33. **Benson NC**, **Butt OH**, **Datta R**, **Radoeva PD**, **Brainard DH**, **Aguirre GK.** The retinotopic organization of striate cortex is well predicted by surface topology. *Curr Biol* 22: 2284, 2012. doi:10.1016/j.cub.2012.11.020.
34. **Benson NC**, **Butt OH**, **Brainard DH**, **Aguirre GK.** Correction of distortion in flattened representations of the cortical surface allows prediction of V1-V3 functional organization from anatomy. *PLoS Comput Biol* 10: e1003538, 2014. doi:10.1371/journal.pcbi.1003538.
35. **Glover GH.** Overview of functional magnetic resonance imaging. *Neurosurg Clin N Am* 22: 133–139, vii, 2011. doi:10.1016/j.nec.2010.11.001.
36. **Bechtold B**, **Fletcher P**, **Seamusholden, Gorur-Shandilya S.** *bastibe/Violinplot-Matlab: A Good Starting Point*. Zenodo, 2021. doi:10.5281/zenodo.4559847.
37. **Cox RW.** AFNI: software for analysis and visualization of functional magnetic resonance neuroimages. *Comput Biomed Res* 29: 162–173, 1996. doi:10.1006/cbmr.1996.0014.
38. **Cox RW**, **Hyde JS.** Software tools for analysis and visualization of fMRI data. *NMR Biomed* 10: 171–178, 1997. doi:10.1002/(sici)1099-1492(199706/08)10:4/5<171::aid-nbm453>3.0.co;2-l.
39. **Saad ZS**, **Reynolds RC.** SUMA. *Neuroimage* 62: 768–773, 2012. doi:10.1016/j.neuroimage.2011.09.016.
40. **Cope TE**, **Baguley DM**, **Griffiths TD.** The functional anatomy of central auditory processing. *Pract Neurol* 15: 302–308, 2015. doi:10.1136/practneurol-2014-001073.
41. **Yetkin FZ**, **Roland PS**, **Mendelsohn DB**, **Purdy PD.** Functional magnetic resonance imaging of activation in subcortical auditory pathway. *Laryngoscope* 114: 96–101, 2004. doi:10.1097/00005537-200401000-00017.
42. **Kastner S**, **Schneider KA**, **Wunderlich K.** Beyond a relay nucleus: neuroimaging views on the human LGN. *Prog Brain Res* 155: 125–143, 2006. doi:10.1016/S0079-6123(06)55008-3.
43. **Schneider KA**, **Richter MC**, **Kastner S.** Retinotopic organization and functional subdivisions of the human lateral geniculate nucleus: a high-resolution functional magnetic resonance imaging study. *J Neurosci* 24: 8975–8985, 2004. doi:10.1523/JNEUROSCI.2413-04.2004.
44. **Zenger-Landolt B**, **Heeger DJ.** Response suppression in v1 agrees with psychophysics of surround masking. *J Neurosci* 23: 6884–6893, 2003. doi:10.1523/JNEUROSCI.23-17-06884.2003.
45. **McAlonan K**, **Cavanaugh J**, **Wurtz RH.** Guarding the gateway to cortex with attention in visual thalamus. *Nature* 456: 391–394, 2008. doi:10.1038/nature07382.
46. **Kimura A**, **Yokoi I**, **Imbe H**, **Donishi T**, **Kaneoke Y.** Auditory thalamic reticular nucleus of the rat: anatomical nodes for modulation of auditory and cross-modal sensory processing in the loop connectivity between the cortex and thalamus. *J Comp Neurol* 520: 1457–1480, 2012. doi:10.1002/cne.22805.
47. **Kimura A.** Diverse subthreshold cross-modal sensory interactions in the thalamic reticular nucleus: implications for new pathways of cross-modal attentional gating function. *Eur J Neurosci* 39: 1405–1418, 2014. doi:10.1111/ejn.12545.
48. **Sherman SM**, **Koch C.** The control of retinogeniculate transmission in the mammalian lateral geniculate nucleus. *Exp Brain Res* 63: 1–20, 1986. doi:10.1007/BF00235642.
49. **Smith AT**, **Williams AL**, **Singh KD.** Negative BOLD in the visual cortex: evidence against blood stealing. *Hum Brain Mapp* 21: 213–220, 2004. doi:10.1002/hbm.20017.
50. **Shmuel A**, **Yacoub E**, **Pfeuffer J**, **Moortele P**, **Adriany G**, **Hu X**, **Uğurbil K.** Sustained negative BOLD, blood flow and oxygen consumption response and its coupling to the positive response in the human brain. *Neuron* 36: 1195–1210, 2002. doi:10.1016/s0896-6273(02)01061-9.
51. **Kobayashi Y**, **Isa T.** Sensory-motor gating and cognitive control by the brainstem cholinergic system. *Neural Netw* 15: 731–741, 2002. doi:10.1016/s0893-6080(02)00059-x.
52. **Molnár Z**, **Belgard TG.** Transcriptional profiling of layers of the primate cerebral cortex. *Neuron* 73: 1053–1055, 2012. doi:10.1016/j.neuron.2012.03.007.
53. **Gut NK**, **Winn P.** The pedunculopontine tegmental nucleus—a functional hypothesis from the comparative literature. *Mov Disord* 31: 615–624, 2016. doi:10.1002/mds.26556.
54. **Woolsey TA**, **Rovainen CM**, **Cox SB**, **Henegar MH**, **Liang GE**, **Liu D**, **Moskalenko YE**, **Sui J**, **Wei L.** Neuronal units linked to microvascular modules in cerebral cortex: response elements for imaging the brain. *Cereb Cortex* 6: 647–660, 1996. doi:10.1093/cercor/6.5.647.
55. **Harel N**, **Lee SP**, **Nagaoka T**, **Kim DS**, **Kim SG.** Origin of negative blood oxygenation level-dependent fMRI signals. *J Cereb Blood Flow Metab* 22: 908–917, 2002. doi:10.1097/00004647-200208000-00002.
56. **Goense J**, **Bohraus Y**, **Logothetis NK.** FMRI at high spatial resolution: implications for BOLD-models. *Front Comput Neurosci* 10: 66, 2016. doi:10.3389/fncom.2016.00066.
57. **Shmuel A**, **Augath M**, **Oeltermann A**, **Logothetis NK.** Negative functional MRI response correlates with decreases in neuronal activity in monkey visual area V1. *Nat Neurosci* 9: 569–577, 2006. doi:10.1038/nn1675.
58. **Kubota M**, **Sugimoto S**, **Hosokawa Y**, **Ojima H**, **Horikawa J.** Auditory-visual integration in fields of the auditory cortex. *Hear Res* 346: 25–33, 2017. doi:10.1016/j.heares.2017.01.012.
59. **Tse PU**, **Baumgartner FJ**, **Greenlee MW.** Event-related functional MRI of cortical activity evoked by microsaccades, small visually-guided saccades, and eyeblinks in human visual cortex. *Neuroimage* 49: 805–816, 2010. doi:10.1016/j.neuroimage.2009.07.052.
60. **Iurilli G**, **Ghezzi D**, **Olcese U**, **Lassi G**, **Nazzaro C**, **Tonini R**, **Tucci V**, **Benfenati F**, **Medini P.** Sound-driven synaptic inhibition in primary visual cortex. *Neuron* 73: 814–828, 2012. doi:10.1016/j.neuron.2011.12.026.
61. **Huber L**, **Goense J**, **Kennerley AJ**, **Trampel R**, **Guidi M**, **Reimer E**, **Ivanov D**, **Neef N**, **Gauthier CJ**, **Turner R**, **Möller HE.** Cortical lamina-dependent blood volume changes in human brain at 7 T. *Neuroimage* 107: 23–33, 2015. doi:10.1016/j.neuroimage.2014.11.046.
62. **Yu Y**, **Huber L**, **Yang J**, **Jangraw DC**, **Handwerker DA**, **Molfese PJ**, **Chen G**, **Ejima Y**, **Wu J**, **Bandettini PA.** Layer-specific activation of sensory input and predictive feedback in the human primary somatosensory cortex. *Sci Adv* 5: eaav9053, 2019. doi:10.1126/sciadv.aav9053.
63. **Fracasso A**, **Luijten PR**, **Dumoulin SO**, **Petridou N.** Laminar imaging of positive and negative BOLD in human visual cortex at 7 T. *Neuroimage* 164: 100–111, 2018. doi:10.1016/j.neuroimage.2017.02.038.